ELSEVIER

Journal of Magnetism and Magnetic Materials 187 (1998) 1–11

Journal of magnetism and magnetic materials

Exchange coupling of Co/Cr(0 0 1) superlattices for in-plane and perpendicular anisotropy

Th. Zeidler*, K. Theis-Bröhl, H. Zabel

Fakultät für Physik und Astronomie, Institut für Experimentalphysik/Festkörperphysik, Ruhr-Universität Bochum, D 44780 Bochum, Germany

Received 2 January 1998

Abstract

We have investigated the exchange coupling of Co/Cr(0 0 1) superlattices by polar and longitudinal magneto-optical Kerr effect measurements, by varying both the Co and Cr film thicknesses. At a Co thickness of ≈ 10 Å a nearly perpendicular anisotropy is found with antiferromagnetic order in the range of 5–15 Å of Cr thickness. For these superlattices the magnetization curve starting from remanence to saturation is characterized by a surface spin-flip transition at low field, followed by domain wall nucleation and motion, and finally by a coherent spin rotation with increasing field. Antiferromagnetic coupling is also observed for superlattices with thicker Co layers and with in-plane magnetic anisotropy.

Keywords: Exchange coupling; Superlattices; Anisotropy – perpendicular; Anisotropy – in-plane

1. Introduction

There has been much interest in recent years in the magnetic properties of Fe/Cr(0 0 1) superlattices. The most important discoveries include the observation of a magnetic exchange coupling [1], a long-period oscillatory exchange coupling as a function of the Cr layer thickness [2,3] superposed on a shorter two monolayer oscillation period [4,5], a non-collinear contribution to the exchange coupling [6–8], and a giant magnetoresistance effect [9,10]. In comparison, Co/Cr(0 0 1) superlattices have received much less attention. Nevertheless, it would be of considerable interest to compare the coupling period, phase and amplitude of the exchange coupling in Fe/Cr and Co/Cr superlattices. The somewhat lower interest in Co/Cr is, in part, due to the mismatched crystal structures and the complex epitaxial relationship between Co and Cr. While both Fe and Cr have a BCC structure with a lattice mismatch of less than 0.4%, the equilibrium crystal structure of Co is HCP. The first few monolayers of Co grow with a pseudomorphic BCC structure on Cr(0 0 1) rotated by 45° with respect to the Cr[1 0 0] in-plane axis [11–13]. With increasing Co thickness the structure relaxes back continuously into the intrinsic HCP structure with the *c*-axis in the plane parallel to Cr[1 1 0] [11,12]. This lattice relaxation

* Corresponding author.

0304-8853/98/$19.00
PII: S0304-8853(98)00121-8

has a profound effect on the magnetic anisotropy properties of Co/Cr superlattices [14]. For thicker Co layers of 20 Å and more, the easy axis is in the plane due to the shape anisotropy. For thinner Co layers the surface anisotropy contribution dominates the magnetic properties of this system, which is negative for HCP-Co but positive for BCC-Co. Thus, with decreasing Co thickness first the easy axis turns up into the perpendicular direction reaching a maximum at about 10–13 Å. However, before reaching a complete out-of-plane orientation, the magnetization vector drops back into the plane. This re-orientation of the perpendicular anisotropy as a function of the magnetic layer thickness has to be distinguished from re-orientational transitions which can be observed as a function of temperature, for instance, in Fe/Cu [15,16] and Fe/Ag superlattices [17,18]. In contrast, Co/Cr(0 0 1) superlattices offer the unique opportunity to independently tune both, the perpendicular anisotropy and the sign of the exchange coupling by varying either the ferromagnetic or the non-ferromagnetic metal layer thickness, respectively.

For more detailed information on the structure and magnetic anisotropy, we refer to our previous papers [11,12,14,19–22]. Here we present a detailed study of the exchange coupling in Co/Cr(0 0 1) superlattices. We have also extended our previous investigations of the magnetic anisotropy to lower temperatures, which are reported in here.

2. Sample preparation and MOKE set-up

High-quality single crystal Co/Cr(0 0 1) superlattices were grown by molecular beam epitaxy (MBE) at 300–350°C on a buffer system consisting of a Nb(0 0 1) seed layer grown at 900°C on $Al_2O_3(1\,0\,\bar{1}\,2)$-substrates and an additional Cr(0 0 1) buffer layer grown at 450°C with thicknesses t_{Nb}, $t_{Cr} \approx 500$ Å. For the study of the exchange coupling and anisotropy, we have grown Co/Cr(0 0 1) superlattices with specific thicknesses for the Co and the Cr layers as well as superlattices with a wedge-type Cr layer between the Co layers of constant thickness. The wedged superlattices are more convenient for comparative studies of the strength of the exchange coupling, whereas the superlattices with fixed layer thicknesses were used for the study of spin structures and magnetization processes. The Co thicknesses were chosen between $t_{Co} \approx 5$–30 Å and in the wedged samples the Cr–thicknesses varied from $t_{Cr} \approx 5$–25 Å and from ≈ 12–19 Å.

We have studied the exchange coupling in Co/Cr(0 0 1) superlattices via the magneto-optical Kerr effect (MOKE) using a set-up described in more detail in Ref. [14]. With a Faraday modulator and lock-in techniques we achieve angular resolutions of $\leqslant 10^{-4^\circ}$. The plane of polarization of the He–Ne laser beam ($\lambda = 632.8$ nm, $P = 5$ mW) was aligned perpendicular to the plane of incidence (s state). In the polar configuration, used for samples with perpendicular anisotropy, the angle of incidence was smaller than 2°.

At room temperature, magnetic fields up to 18 kOe are available. For low-temperature work down to $T = 4.2$ K we used a cryostat as shown in Fig. 1 with a superconducting magnet providing fields up to 30 kOe. An experimental problem constitutes the optical windows for low temperature studies. Windows without changes of the optical birefringence exist only at room temperature. Therefore, we avoided any optical windows inside of the cryostat and the sample was positioned outside of the inner cryostat, as indicated in Fig. 1. Liquid He flow through the inner part guaranteed

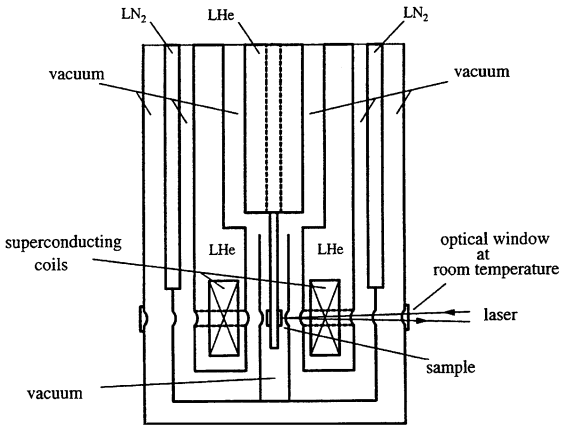

Fig. 1. Schematic outline of the He cryostat used for polar MOKE–measurements at low temperatures.

satisfactory heat contact. The outside window also causes problems since it produces a Faraday effect proportional to the applied magnetic field yielding an additional linear contribution to the MOKE signal. All measurements shown here have been corrected for these effects.

3. Phenomenological anisotropy energy model

For the analysis of the magnetic anisotropy and the interlayer exchange coupling of Co/Cr(0 0 1) superlattices we have performed absolute minima calculations of the phenomenological energy density E, including terms for the Zeeman energy, shape anisotropy, crystal anisotropies of second and forth order of HCP-Co, K_2 and K_4, respectively, and an interface anisotropy constant K_S. For the polar configuration we use the expression:

$$\begin{aligned} E = & -\sum_{n=1}^{N} \mu_0 M_S H \cos(\theta_n - \theta_H) \\ & + \frac{1}{2}\sum_{n=1}^{N} \mu_0 M_S^2 \cos^2\theta_n \\ & + \sum_{n=1}^{N} K_2 \cos^2\theta_n + \sum_{n=1}^{N} K_4 \cos^4\theta_n \\ & + \sum_{n=1}^{N} \frac{1}{t_{Co}} 2K_S \cos^2\theta_n + \sum_{n=1}^{n} K_U \cos^2(\theta_n - \theta_U) \\ & + \sum_{n=1}^{N-1} \frac{J_{AF}}{t_{Co}} \cos(\theta_n - \theta_{n+1}), \end{aligned} \tag{1}$$

here t_{Co} is the thickness of the Co layer. The angle θ_n ($n = 1..N$, N = number of Co layers) is defined as the angle between the sample normal and the orientation of the magnetization vector in the layers of the superlattice. The magnetic field H is applied perpendicular to the surface with $\theta_H = 0$. The saturation magnetization M_S is assumed to be homogeneous in each Co layer. An additional uniaxial anisotropy contribution is introduced via K_U with an arbitrary orientation θ_U with respect to the sample normal. The need for this anisotropy term will be justified later. The AFM coupling term prefers an antiparallel orientation of adjacent Co layers for $J_{AF} < 0$.

If all anisotropy contributions are known, a fit of the calculated magnetization $M(H)$ loop according to Eq. (1) and

$$\frac{M}{M_S} = \frac{1}{N}\sum_{n=1}^{N} \cos\theta_n \tag{2}$$

to the experimental points is possible and produces quantitative values for the coupling term J_{AF}.

4. Magnetic anisotropy properties of Co/Cr(0 0 1)

For the analysis of the interlayer exchange coupling a knowledge of the anisotropy properties is indispensable. The room temperature results can be summarized as follows [14,19,20]. An interface anisotropy constant $K_S \approx -0.65\,\mathrm{mJ/m^2}$ causes a transition of the orientation of the magnetization vector from in–plane to the out–of–plane direction with decreasing Co thickness t_{Co}. Extrapolation of the anisotropy field as a function of the inverse Co layer thickness yields the critical thickness for the reorientation of $t_{Co}^{crit} \approx 13.5$ Å. The rotation of the easy axis stops at an angle θ of $\approx 75^\circ$, and for $t_{Co} < 12$ Å the easy axis turns back into the plane. This most remarkable effect is governed by the concomitant structural phase transition of the Co layers from hcp to bcc with decreasing Co thickness, which, in turn, causes a sign change of the interface anisotropy constant K_S.

By minimizing Eq. (1) and fitting to the measured MOKE hysteresis curves we find the other crystal anisotropy constants: $K_2 \approx 2.1 \times 10^5\,\mathrm{J/m^3}$ and $K_4 \approx 1.1 \times 10^5\,\mathrm{J/m^3}$. The value for K_2 is slightly smaller than typical values reported in the literature [23–25], but remains of the same order of magnitude.

In the Co layer thickness regime of the reorientational transition an additional anisotropy constant K_U is required, which defines a canted orientation for the magnetization vector θ_U according to Eq. (1). Introducing this anisotropy constant is justified by the experimental results shown in Fig. 2, which reveal a hard axis if the magnetic field is applied with an angle of 15° to the sample surface (see inset of the figure). This indicates that a canted easy axis exists with an orientation of about

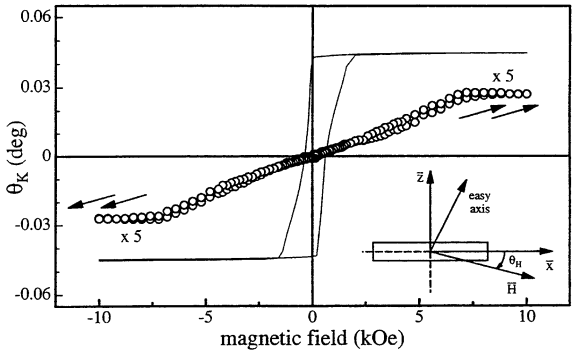

Fig. 2. Hard-and easy-axis hysteresis loops for a Co/Cr(0 0 1) superlattice with $t_{Co} = 12$ Å and measured in the polare MOKE configuration at room temperature. The circles show a hysteresis with the magnetic field applied along a direction 105° away from the perpendicular direction as indicated in the inset. The solid line shows the appertaining MOKE curve along the easy axis at an angle of 15° with respect to the normal.

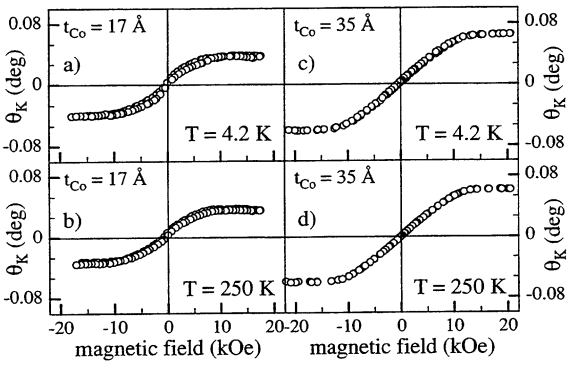

Fig. 3. Polar MOKE measurements of Co/Cr(0 0 1) superlattices for Co thicknesses $t_{Co} \geqslant 17$ Å at $T = 4.2$ K and near room temperature. No significant temperature dependence of the hysteresis loops is observable.

$\theta_U = 15°$ away from the normal direction and for $t_{Co} = 12$ Å. By the shape of the hard axis loop in Fig. 2 it is clear that no sixth- or higher-order anisotropy term is required for the description of the magnetic anisotropy of this system. From the observed saturation field of $H_{sat} \approx 7.2$ kOe and a slightly reduced value for the saturation magnetization $M_S = 10^6$ A/m[14], we determine the uniaxial anisotropy constant to $K_U \approx 2.8 \times 10^5$ J/m^3. The origin of K_U is not clear at present. It may be related to the substrate and buffer layer miscut in the present superlattices. In any case, the K_U is required for a phenomenological description of the anisotropy and the coupling behavior for Co layer thicknesses smaller than 14 Å.

We are now turning to our low-temperature results. We were interested in the temperature dependence of the anisotropy constants K_2 and K_4, and the question, whether at low temperatures another re-orientational transition of the anisotropy occurs, as reported previously for the Fe/Cu [15,16], the Fe/Ag [17,18], and most recently also for the Co/Ho interfaces [26].

First, we compare magnetic hysteresis curves recorded at high (250 K) and low temperatures (4.2 K) and for two different Co thicknesses of 17 and 35 Å for which the easy axis is in the plane. The Cr thickness of 20 Å is chosen such that the exchange coupling is rather weak. The polar MOKE measurements are taken with the magnetic field applied along the hard axis. As shown in Fig. 3, there is no significant change of the magnetization curve at high and low temperatures. This is a rather surprising result, which is clearly inconsistent with the temperature dependence known for bulk HCP Co [23]. In bulk Co, the crystal anisotropy constant K_2 increases by about 40% between room temperature and 70 K, while K_4 remains nearly constant. One would expect a similar temperature dependence also to be present for Co/Cr(0 0 1) superlattices with thickner Co layers, which, however, is clearly not the case.

For Co thicknesses in the range of the perpendicular anisotropy ($t_{Co} < 12$ Å), the magnetic anisotropy is also nearly temperature independent. The polar MOKE measurements reproduced in Fig. 4 show that only the coercive fields and the remanent Kerr rotation increases slightly at $T = 4.2$ K.

For both anisotropies, the MOKE data clearly show that no further reorientation of the easy axis as a function of temperature takes place. Therefore, the reorientational transition is solely induced by the structural transition of the Co layer from HCP to pseudo-BCC with decreasing thickness.

It is well known that the magneto-crystalline anisotropy depends sensitively on crystal field and band structure properties. In particular, the Co

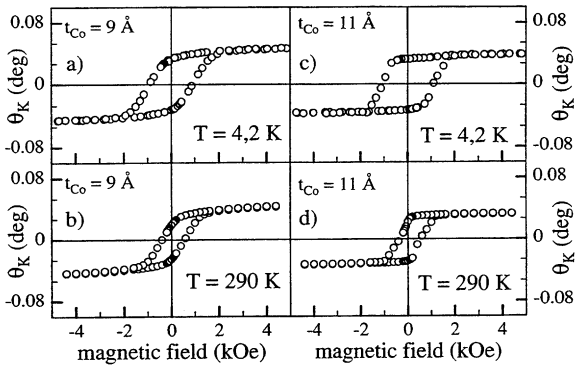

Fig. 4. Polar MOKE measurements of Co/Cr(0 0 1) superlattices with different Co thicknesses $t_{Co} \leqslant 14$ Å at $T = 4.2$ K and near room temperature. Aside from slightly increased coercive fields at low temperatures, no significant temperature dependence of the hysteresis loops is observable.

anisotropy constant K_2 depends strongly on small changes of the c/a ratio for the HCP lattice constants. Due to epitaxial strains and pseudomorphic growth of the Co layers in Co/Cr(0 0 1) superlattices, we expect the magneto-elastic contribution of the anisotropy to deviate from its bulk counterpart and, furthermore, to be temperature dependent. At present the temperature dependence of the c/a ratio for Co/Cr superlattices is not known. The temperature-independent hysteresis curves seem, however, to indicate that the c/a ratio remains constant with decreasing temperature.

5. Exchange coupling in Co/Cr(0 0 1) superlattices

5.1. Exchange coupling with perpendicular anisotropy

In the following we report room temperature results on the exchange coupling in Co/Cr(0 0 1) superlattices and for Co thicknesses ($t_{Co} \approx 10$ Å) exhibiting perpendicular anisotropy. Hysteresis loops were taken along a wedged superlattice with Cr layer thickness increasing between 5 and 25 Å. A typical hysteresis loop is reproduced in Fig. 5 for a Cr thickness of 13 Å. Here we clearly observe an antiferromagnetically (AFM) coupled superlattice close to perpendicular anisotropy. The shape of the hysteresis curve and the resulting spin structure will

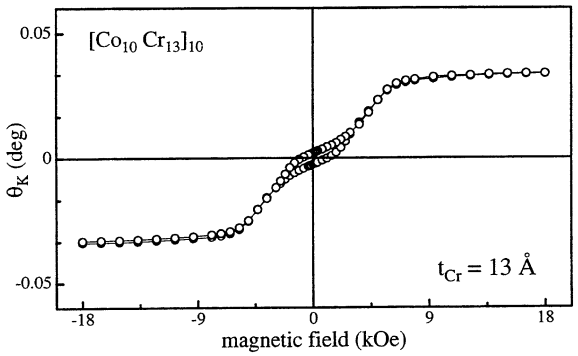

Fig. 5. The polar MOKE hysteresis curve of Co/Cr(0 0 1) superlattices with $t_{Cr} \leqslant 13$ Å exhibits an AF coupling. The slope in the remnant regime is due to a uniaxial anisotropy with a canted easy axis with respect to the layer normal.

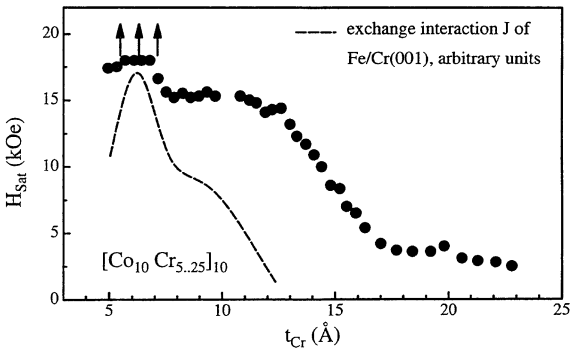

Fig. 6. Polar saturation field H_{sat} as a function of Cr layer thickness. The superlattices are not saturated in the area around $t_{Cr} \approx 6$ Å in magnetic fields up to 18 kOe. The dashed line reproduces the position and shape of the saturation field in Fe/Cr(0 0 1) superlattices around the first AF maximum according to Ref. [22].

be explained in detail further below. The saturation field, which is a measure of the coupling strength, is plotted as a function of the Cr layer thickness in Fig. 6.

The first maximum of the AFM interlayer coupling occurs at $t_{Cr} \approx 6$ Å. Using Eq. (1) and the anisotropy parameters as discussed in Section 4, a coupling strength of $|J_{AF}| > 0.5\ \mathrm{mJ/m^2}$ is evaluated. We can provide only a lower limit for the coupling strength since we could not saturate the sample in the polar configuration with fields up to 18 kOe.

Our results should be compared with earlier experiments by Parkin on polycrystalline Co/Cr multilayers [27]. In the latter case a first AFM maximum is observed at 7 Å with a coupling strength of 0.24 mJ/m^2. Both values are in fair agreement with our results, considering the different growth methods and structures. According to the earlier experiments, the second long period maximum occurs at 25 Å which is outside of the thickness range investigated here. The shape, position, and strength of the saturation field as a function of the Cr layer thickness in Co/Cr(0 0 1) is also in rather good agreement with the Fe/Cr(0 0 1) results for the long period exchange coupling (dashed line in Fig. 6) [3].

5.2. Magnetic hysteresis of exchange coupled superlattices with perpendicular anisotropy

Sandwich structures with a uniaxial anisotropy K_U and an interlayer antiferromagnetic coupling ($J_{AF} < 0$) exhibit a spin structure as a function of an external field which is usually completely symmetric. Therefore, the magnetic hysteresis is expected to be symmetric as well, as shown schematically in Fig. 7. If $K_U < J_{AF}/t_m$, where t_m is the thickness of the magnetic layers, a coherent rotation of the spins occurs, as shown in Fig. 7a. In the opposite case of $K_U > J_{AF}/t_m$, a spin flip transition at the field $H_F = H_S$ dominates the magnetization process, as shown in Fig. 7b.

Fig. 8 reproduces the polar MOKE hysteresis measurement (open circles) of an antiferromagnetically coupled Co/Cr(0 0 1) superlattice with $N = 10$ magnetic double layers. The wide range of a nearly zero remanent magnetization and the high saturation field are characteristic of the strong coupling in this superlattice. As mentioned above, at $t_{Co} = 12$ Å, the easy axis is slightly slanted with respect to the perpendicular orientation. Because of this, the MOKE curves in Fig. 8 and also in Fig. 5 exhibit a significant slope in the field range between $H = 0$ and $H = H_1$. Comparing the schematics in Fig. 7 with the experimental results as shown in Fig. 8, we can qualitatively conclude that the magnetic hysteresis is characterized by coherent spin rotation. Details of the spin structure will, however, follow from a more quantitative analysis via a fit to the hysteresis curve, as discussed below.

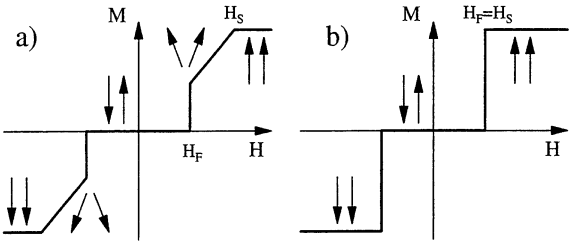

Fig. 7. Symmetric spin orientation of a magnetic sandwich system during the remagnetization process. In (a) coherent spin rotation is dominant wheras in (b) only spin flip transitions occur.

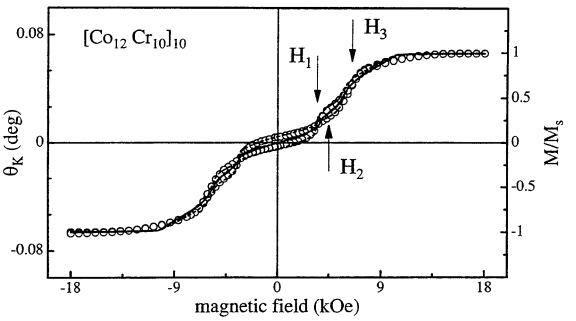

Fig. 8. Polar MOKE measurement of an AF coupled Co/Cr(0 0 1) superlattice (open circles) and the theoretical magnetization curve using Eq. (1) (solid line). The theoretical MOKE curve is plotted by dashed lines. For more details see text.

Close to remanence a crossing of the magnetization curves can be recognized. This is due to the fact that the top magnetic layer of the superlattice contributes mainly to the MOKE signal, whereas for the inner layers the MOKE sensitivity decreases exponentially. Neglecting depth-dependent MOKE sensitivity, our fit to the MOKE curve shown by the solid line in Fig. 8 is in excellent agreement with the experimental data.

The model calculation is based on Eq. (1) and the parameters are listed in Table 1. We have calculated the hysteresis loop according to the classical Maxwell theory for magnetic multilayers with arbitrary orientation of the magnetization vector θ_n following the treatment of Moog et al. [28–31]. For the optical and magneto-optical constants of

Table 1
Magnetic anisotropy and coupling parameters used to fit the magnetic hysteresis in Fig. 8 according to the model described in Eq. (1)

M_S (kA/m)	K_1 (J/m^3)	K_2 (J/m^3)	K_S (mJ/m^2)	K_U (J/m^3)	θ_U (deg)	J_{AF} (mJ/m^2)	t_{Co} (Å)
1000	2.1×10^5	1.1×10^5	-0.65	1.8×10^5	30	-0.33	12

Co and Cr we used literature values from Refs. [32,33].

According to our model calculation, the spin structure of the Co/Cr(0 0 1) superlattice with 10 double layers is highly asymmetric at low fields, explaining the rather complicated hysteresis loop in Fig. 8. In remanence the magnetic moments are oriented antiparallel along the easy-axis direction, as indicated schematically in Fig. 9a, including the canted easy axis. With increasing field, a surface spin flip transition with a domain wall nucleation takes place at H_1 and leads to an asymmetric spin structure (Fig. 9b). At slightly higher fields, H_2, we observe a 'domain wall' motion to a more stable state. The spins are now oriented symmetrically with respect to the center of the superlattice (Fig. 9c). For $H > H_3$, all spins switch into the field direction. Finally, a coherent rotation of the layer magnetization takes place until saturation is reached. The two outermost Co layers differ slightly in their orientation from the inner layers, since they are coupled to only one neighbor each.

In Fig. 10 we show another example for perpendicular anisotropy and spin rotation in exchange coupled Co/Cr superlattices as determined by polar MOKE measurements. Here the hysteresis is characterized by a spin flip transition, according to Fig. 7b. Again the MOKE curves cross close to remanence due to magneto-optical effects. In principle, the finite Kerr rotation in remanence could be explained by a non-collinear spin structure containing biquadratic coupling terms. However, additional investigations with polarized neutron reflectivity provided no evidence for this assumption [34].

The calculated magnetization curve using Eq. (1) is shown by a solid line in Fig. 10. The corresponding layer magnetization vectors are schematically reproduced in Fig. 11. Starting from the remanent magnetization (Fig. 11a), a surface spin flip transition occurs again at very low fields, which is, however, extremely unstable. With a slight increase of the field up to H_1, the spin structure becomes symmetric with respect to the center of the superlattice (Fig. 11b). A second spin flip transition occurs at H_2 and leads to saturation without any further intermediate states (Fig. 11c). The fit

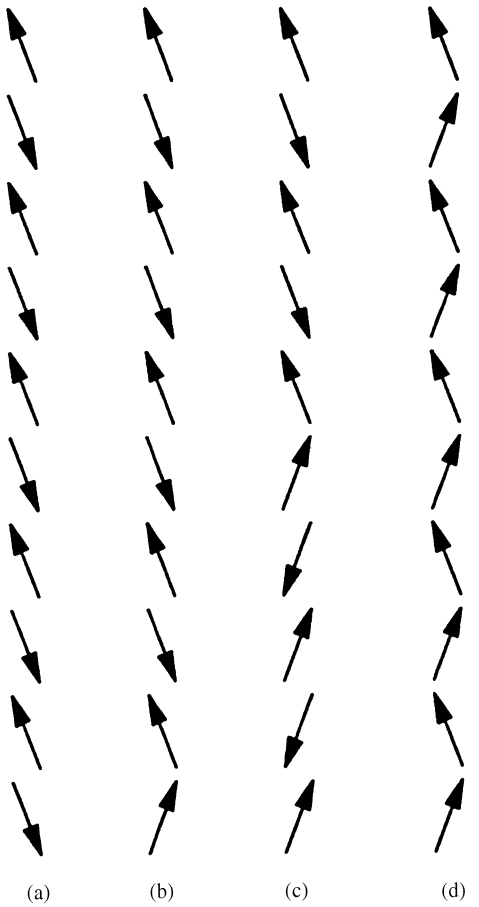

Fig. 9. Spin structure of an AF coupled Co/Cr(0 0 1) superlattice for different magnetic fields. More details are provided in the text.

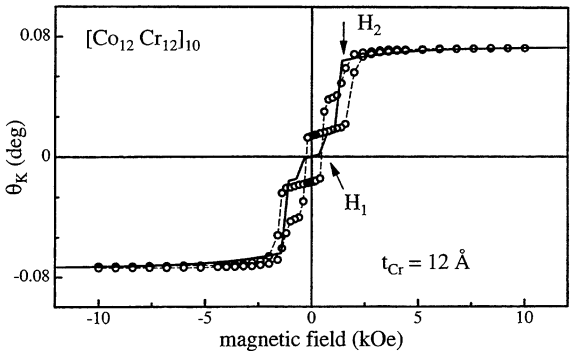

Fig. 10. Polar MOKE measurement of an AF coupled Co/Cr(0 0 1) superlattice (open circles) and the theoretical magnetization curve using Eq. (1) (solid line).

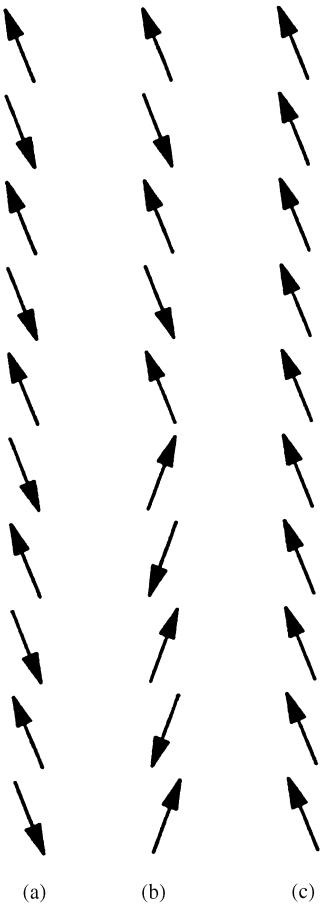

Fig. 11. Spin structure of an AF coupled Co/Cr(0 0 1) superlattice for different magnetic fields. More details are given in the text.

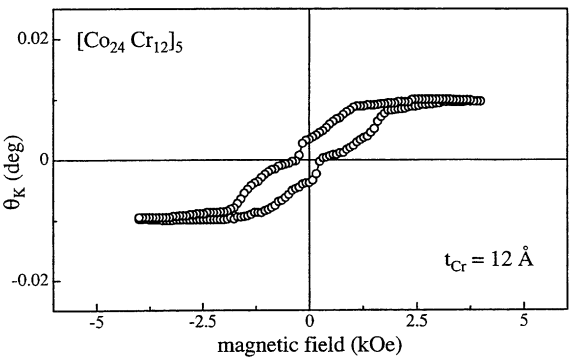

Fig. 12. Longitudinal MOKE hysteresis loop of an AFM coupled superlattice with $t_{Cr} = 12$ Å. The superlattice comprises an odd number of periods, such that the magnetization is not completely cancelled in remanence.

yields a rather weak AFM coupling constant of $J_{AFM} \approx -0.07\ \mathrm{mJ/m^2}$.

5.3. Exchange coupling with in-plane anisotropy

We have also investigated the exchange coupling for Co thicknesses with in-plane anisotropy. Longitudinal MOKE measurements were carried out using wedged sample with a constant Co thickness of 22 Å and with Cr thicknesses varying between 12–19 Å.

In Fig. 12 we show a hysteresis loop taken with the longitudinal MOKE configuration and for a superlattice having five periods of thicknesses $t_{Co} = 22$ and $t_{Cr} = 12$ Å, respectively. The odd number of magnetic layers prevents the magnetization from complete cancellation at remanence even in the case of a perfect AFM coupling. The dependence of the saturation field as a function of the Cr thickness is plotted in Fig. 13. A very high saturation field is observed at about 12 Å. However, the maximum may occur at even smaller Cr thickness, in agreement with the out-of-plane coupling. From the saturation field and the known anisotropy constants we derive an exchange coupling constant $J_{AF} \approx -0.3\ \mathrm{mJ/m^2}$.

5.4. Temperature dependence of the exchange coupling

We have also measured the low-temperature magnetic hysteresis of samples with perpendicular

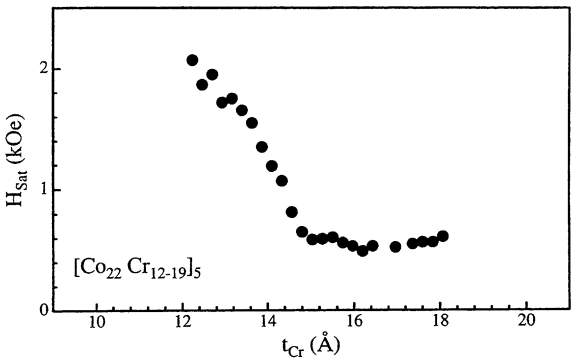

Fig. 13. Saturation fields H_{Sat} from longitudinal MOKE measurements are plotted as a function of the Cr thickness. The results are qualitatively in good agreement with exchange coupling in the perpendicular orientation.

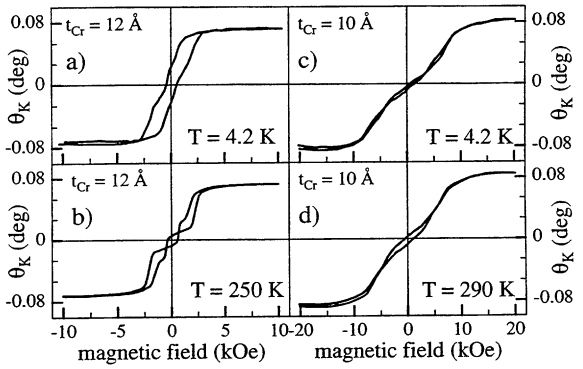

Fig. 14. Polar MOKE measurements of AF coupled Co/Cr(0 0 1) superlattices with different Cr layer thicknesses are compared for temperatures of 4.2 and 250 (290) K. The temperature dependence is not dramatic, indicating that neither the anisotropy nor the exchange coupling depend strongly on the temperature.

anisotropy (Co thickness ≈ 10 Å). In Fig. 14 we compare polar MOKE curves taken at 4.2 K with measurements at higher temperatures. For the sample with $t_{Cr} = 10$ Å we observe a coherent spin rotation with very little temperature dependence (Fig. 14c and d). However, a strong temperature dependence of the magnetization curve can be recognized for the sample with weak AFM coupling ($t_{Cr} = 12$ Å) as shown in Fig. 14a and b. Nevertheless, the saturation field remains unchanged indicating no significant temperature dependence of the coupling term J_{AFM}, in agreement with coupling theories. The hysteresis changes shape between the flip fields $-H_2 < H < +H_2$, which is caused by an increased number of pinning centers for domain wall motion. This stretches out and rounds off the descrete jumps in the hysteresis loops with decreasing temperature.

6. Discussion and summary

One important result of the present investigation is the observation that the interlayer exchange coupling in Co/Cr(0 0 1) superlattices is in principal agreement with the exchange coupling in Fe/Cr(0 0 1) superlattices respecting the amplitude and the phase of the first AFM maximum. The magnetic exchange splitting of bulk Co and Fe are comparable and, according to the theory of quantum well states (QWS), prefer similar phases for the interlayer coupling [35–38]. In contrast to Fe/Cr(0 0 1), so far we have not been able to observe a second AFM maximum nor a two ML oscillation period. Some indications for a 2 ML short period oscillation have been found in asymmetric trilayer structures of Co/Cr/Fe(0 0 1) [22].

Some information on the exchange coupling of Co/Cr(0 0 1) superlattices with in-plane anisotropy is also available from other groups. Harp and Parkin [39] observed AFM coupling for a superlattice with a Cr thickness of 10 Å, whereas for 12 Å Cr thickness they report ferromagnetic coupling. However, their 12 Å sample shows a remanent magnetization which is considerably reduced compared to the saturation magnetization, indicative of AFM or biquadratic contributions at this Cr thickness. Picconatto et al. [40] investigated a Co(20 Å)/Cr(10 Å) superlattice, exhibiting a hysteresis with a clear AFM coupling. They derive an exchange coupling constant of $|0.55|\ mJ/m^2$, in good agreement with our results. Recently, Aliev et al. [41] have investigated Co/(Cr/Ag)/Co superlattices with Cr/Ag bilayers as non-ferromagnetic spacer layers. The Co thickness of 45 Å guarantees an in-plane easy axis. Below 7 Å they observe ferromagnetic coupling, whereas AFM coupling occurs between 10 − 23 Å with a very broad maximum. A second AFM peak was not observed.

Our polar MOKE measurements and the simulations do not require a second-order biquadratic coupling term of the form $J_2/t_{Co}\cos^2(\theta_n - \theta_{n-1})$, as for Fe/Cr(0 0 1). Using such a term in our simulation does not improve the fits to the experimental points.

Another important aspect of our investigations concerns the magnetic hysteresis for perpendicular anisotropy in an external magnetic field. The two cases of magnetization curves known for trilayers can also be observed in the superlattices. In the former case, saturation will be reached either via a coherent spin rotation or by spin flip processes depending on the ratio of the magnetic anisotropy and the exchange coupling. In either case, the spin structure is symmetric over the entire remagnetization process. In contrast, superlattices exhibit naturally a much more asymmetric spin structure during remagnetization due to surface spin flips and domain wall motions. A surface spin-flip transition and domain wall motion has also been observed in Fe/Cr(2 1 1) superlattices [42]. Note that the surface spin-flip transition is just due to the chosen boundary condition. Magnetization calculations for a superlattice with periodic boundary conditions show only a coherent spin rotation without any domain wall nucleation.

At low temperatures, the magnetic hysteresis of exchange coupled Co/Cr(0 0 1) superlattices does not change in a dramatic way. This indicates that on the one hand the coupling strength remains constant at low temperatures in agreement with the theory, and on the other a temperature-induced reorientation of the magnetic anisotropy does not take place even for $t_{Co} < 14$ Å, in agreement with the temperature-independent anisotropy constants.

In summary, we have measured via longitudinal and polar Kerr effect measurements the exchange coupling in Co/Cr(0 0 1) superlattices. Depending on the Co thickness, the exchange coupling may occur either with spins in or out of the plane. For both spin orientations, antiferromagnetic exchange coupling exists over a broad region of Cr thicknesses from 5 to 15 Å. Low temperature measurements show that neither the anisotropy parameters nor the exchange coupling depend on the temperature.

Acknowledgements

We would like to thank W. Donner for the MBE growth of the Co/Cr superlattices, and J. Podschwadek and W. Oswald for their technical assistance. The work in Bochum was supported by the DFG through SFB 166 “Structural and magnetic phase transitions.”

References

[1] P. Grünberg, R. Schreiber, Y. Pang, M.B. Brodsky, H. Sowers, Phys. Rev. Lett. 57 (1986) 2442.
[2] S.S.P. Parkin, N. More, K.P. Roche, Phys. Rev. Lett. 64 (1990) 2304.
[3] S. Demokritov, J.A. Wolf, P. Grünberg, Europhys. Lett. 15 (1991) 881.
[4] J. Unguris, R.J. Celotta, D.T. Pierce, Phys. Rev. Lett. 69 (1992) 1125.
[5] J.A. Wolf, Q. Leng, R. Schreiber, P.A. Grünberg, W. Zinn, J. Magn. Magn. Mater. 121 (1993) 253.
[6] M. Rührig, M. Schäfer, A. Hubert, R. Mosler, J.A. Wolf, S. Demokritov, P. Grünberg, Phys. Stat. Solidi (a) 125 (1991) 635.
[7] J.C. Slonczewski, J. Magn. Magn. Mater. 150 (1995) 13.
[8] A. Schreyer, J.F. Ankner, Th. Zeidler, M. Schäfer, H. Zabel, C.F. Majkrzak, P. Grünberg, Europhys. Lett. 32 (1995) 595.
[9] M.N. Baibich, J.M. Broto, A. Fert, F. Nguyen Van Dau, F. Petroff, P. Etienne, G. Creuzet, A. Friederich, J. Chazelas, Phys. Rev. Lett. 61 (1988) 2472.
[10] G. Binasch, P. Grünberg, F. Saurenbach, W. Zinn, Phys. Rev. B 39 (1989) 4828.
[11] W. Donner, N. Metoki, A. Abromeit, H. Zabel, Phys. Rev. B 48 (1993) 14745.
[12] N. Metoki, W. Donner, H. Zabel, Phys. Rev. B 49 (1994) 17351.
[13] J.C.A. Huang, Y.D. Yao, Y. Liou, S.F. Lee, W.T. Yang, C.P. Chang, S.Y. Liao, C.H. Lee, Appl. Surf. Sci. 92 (1996) 480.
[14] Th. Zeidler, F. Schreiber, W. Donner, N. Metoki, H. Zabel, Phys. Rev. B 53 (1996) 3256.
[15] D.P. Pappas, K.P. Kamper, H. Hopster, Phys. Rev. Lett. 64 (1990) 3179.
[16] R. Allenspach, A. Bishof, Phys. Rev. Lett. 70 (1992) 3385.
[17] D.P. Pappas, C.R. Brundle, H. Hopster, Phys. Rev. B 45 (1992) 8169.
[18] Z.Q. Qiu, J. Pearson, S.D. Bader, Phys. Rev. Lett. 70 (1993) 1006.
[19] W. Donner, Th. Zeidler, F. Schreiber, N. Metoki, H. Zabel, J. Appl. Phys. 75 (1994) 6421.
[20] N. Metoki, W. Donner, Th. Zeidler, H. Zabel, J. Magn. Magn. Mater. 126 (1993) 397.

[21] F. Schreiber, Z. Frait, Th. Zeidler, N. Metoki, W. Donner, H. Zabel, J. Pelzl, Phys. Rev. B. 51 (1995) 2929.
[22] K. Theis-Bröhl, R. Scheidt, Th. Zeidler, F. Schreiber, H. Zabel, Th. Mathieu, Ch. Mathieu, B. Hillebrands, Phys. Rev. B 53 (1996) 11 613.
[23] D.M. Paige, B. Szpunar, B.K. Tanner, J. Magn. Magn. Mater. 44 (1984) 239.
[24] F. Ono, J. Phys. Soc. Japan. 50 (1981) 2564.
[25] Z. Frait, Brit. J. Appl. Phys. 15 (1964) 993.
[26] G. Garreau, E. Beaurepaire, M. Farle, J.P. Kappler, Europhys. Lett. 39 (1997) 557.
[27] S.S.P. Parkin, Phys. Rev. Lett. 67 (1991) 3598.
[28] J. Zak, E.R. Moog, C. Liu, S.D. Bader, Phys. Rev. B 43 (1991) 6423.
[29] J. Zak, E.R. Moog, C. Liu, S.D. Bader, J. Appl. Phys. 68 (1990) 4203.
[30] J. Zak, E.R. Moog, C. Liu, S.D. Bader, J. Magn. Magn. Mater. 89 (1990) 107.
[31] E.R. Moog, C. Liu, S.D. Bader, J. Zak, Phys. Rev. B 39 (1988) 6949.
[32] E. Palik, Handbook of Opt. Constants of Solids, Academic Press Handbook Series, New York, 1985.
[33] Z.Q. Qiu, J. Pearson, S.D. Bader, Phys. Rev. B 46 (1992) 8195.
[34] A. Schreyer, private communication.
[35] J.E. Ortega, F.J. Himpsel, G.J. Mankey, R.F. Willis, Phys. Rev. B 47 (1993) 1540.
[36] P. Bruno, J. Magn. Magn. Mater. 116 (1993) L13.
[37] P. Bruno, J. Magn. Magn. Mater. 121 (1993) 248.
[38] M.D. Stiles, Phys. Rev. B 48 (1993) 7238.
[39] G.R. Harp, S.S.P. Parkin, Appl. Phys. Lett. 65 (1994) 3063.
[40] J.J. Picconatto, M.J. Pechan, E.E. Fullerton, J. Appl. Phys. 81 (1997) 5058.
[41] F.G. Aliev, E. Kummen, K. Temst, K. Mae, G. Verbanck, J. Barnas, V.V. Moshchalkov, Y. Bruynseraede, Phys. Rev. Lett. 78 (1997) 134.
[42] R.W. Wang, D.L. Mills, E.E. Fullerton, J.E. Mattson, S.D. Bader, Phys. Rev. Lett. 72 (1994) 920.